International Journal of Biological Macromolecules 274 (2024) 133192

Contents lists available at ScienceDirect

International Journal of Biological Macromolecules

journal homepage: www.elsevier.com/locate/ijbiomac

Hyaluronate loaded advanced wound dressing in form of *in situ* forming hydrogel powders: Formulation, characterization, and therapeutic potential

Chiara Amante [a], Monica Neagu [b], Giovanni Falcone [a], Paola Russo [a], Rita P. Aquino [a], Luigi Nicolais [c], Pasquale Del Gaudio [a,d,*]

[a] Department of Pharmacy, University of Salerno, via Giovanni Paolo II, 132-84084 Fisciano, SA, Italy
[b] Immunology Department, Victor Babes National Institute of Pathology, Bucharest 050096, Romania
[c] Materias s.r.l., University of Naples "Federico II" Campus San Giovanni a Teduccio, Naples, Italy
[d] Research Centre for Biomaterials BIONAM, University of Salerno, 84084 Fisciano, Italy

ARTICLE INFO

Keywords:
Wound healing
Alginate
Pectin
Chitosan
Hyaluronic acid
In situ gelling particles

ABSTRACT

In this paper, a blend composed of alginate-pectin-chitosan loaded with sodium hyaluronate in the form of an *in situ* forming dressing was successfully developed for wound repair applications. This complex polymeric blend has been efficiently used to encapsulate hyaluronate, forming an adhesive, flexible, and non-occlusive hydrogel able to uptake to 15 times its weight in wound fluid, and being removed without trauma from the wound site. Calorimetric and FT-IR studies confirmed chemical interactions between hyaluronate and polysaccharides blend, primarily related to the formation of a polyelectrolytic complex between hyaluronate and chitosan. *In vivo* wound healing assays on murine models highlighted the ability of the loaded hydrogels to significantly accelerate wound healing compared to a hyaluronic-loaded ointment. This was evident through complete wound closure in <10 days, accompanied by fully restored epidermal functionality and no indications of the site of excision or treatment. Therefore, all these results suggest that hyaluronate-loaded powders could be a very promising conformable dressing in several wound healing applications where exudate is present.

1. Introduction

Every year, a great number of people feel pain from planned (*e.g.*, surgery) or accidental (*e.g.*, burns and abrasions) tissue wounds. Wounds can be classified as acute when the injury requires the phases of normal healing (8–12 weeks) and chronic wounds that occur when progress through normal stages of healing (homeostasis, inflammation, migration, proliferation, and maturation) fails and do not respond to treatment over the normally expected healing time frame [1]. Currently, about 1–2 % of the population in developed countries suffers from chronic wounds [2]. The global advanced wound care products market is on the rapid rise with an estimated request of $18.7 billion by 2027 [3]. To date, wound management remains a global medical challenge and it is necessary to treat wounds in the best way. Hydrogels can be successfully used as wound care materials due to their ability to hold a high water content, guarantee a proper moisture environment for the wound [4,5], and control the release of the active ingredients loaded in the wound site [6]. Furthermore, soft hydrogels can be easily removed without pain for the patient [7], and thanks to the transparency of the top layer the healing process can be monitored [8]. Among them, natural polymer-based hydrogels composed of alginate [9], hyaluronic acid [10], and chitosan [11], have received great consideration due to their biocompatibility and three-dimensional porous structure extracellular matrix (ECM) like.

Alginate, a polysaccharide copolymer constituted of -l-guluronic acid (G) and-d-mannuronic acid (M) in repeated units, is widely used and investigated as a wound dressing due to its biocompatibility, biodegradability, and gelling properties [12,13]. Moreover, alginate with a high M content induces cytokine production more than alginate with a high G content [14]. It is, also, able to absorb wound exudates creating a moist environment in the wound bed, and also exhibits hemostatic properties that could be useful for bleeding wounds [15,16]. Other natural polymers can be combined to alginate in order to tune hydrogel properties such as amidated pectin which, gelifing ionotropically when in contact with bivalent cations present in the exudate, enhances the *in situ* gel forming rate [17].

Among polysaccharides for wound dressing applications, chitosan, composed of-1,4-linked glucosamine, and *N*-acetylglucosamine residues

* Corresponding author at: Pasquale Del Gaudio, Department of Pharmacy, University of Salerno, I-84084 Fisciano, SA, Italy.
E-mail address: pdelgaudio@unisa.it (P. Del Gaudio).

https://doi.org/10.1016/j.ijbiomac.2024.133192
Received 11 September 2023; Received in revised form 13 June 2024; Accepted 13 June 2024
Available online 22 June 2024

represents a good candidate for drug delivery due to its numerous biological properties, including excellent bioactivity as hemostatic properties, antimicrobial and anti-inflammatory activity [18–20]. Since the use of dressings based on natural polysaccharides in wound care is limited due to poor mechanical properties and conformability [21,22], a valid alternative to conventional dressings might be *in situ* forming hydrogels composed of polysaccharides that could conform to a wound irregular shape and depth while promoting the healing of the wound. In a previous work [23], we underlined the possibility of using alginate-pectin-chitosan blends to produce *in situ* gelling powders loaded with an antimicrobial drug able to quickly gel when in contact with wound fluids thanks to the formation of polyelectrolyte complex between the protonated amines of the chitosan and the carboxylate groups of the alginate.

In this work, we show how sodium hyaluronate can be loaded into the alginate-pectin-chitosan blend in order to improve the powder technological and healing properties. In fact, hyaluronic acid plays a crucial role in the wound healing process, being a major constituent of ECM, promoting the formation of fibrin clots and the production of interleukins and proinflammatory cytokines. Hyaluronic acid, a linear polyanionic polysaccharide composed of alternating units of a repeating disaccharide D-glucuronic acid and D-*N*-acetyl-d-glucosamine bound with β-glycosidic linkages, is an essential component of the extracellular matrix and exists in connective tissues, skin, and synovial joint fluids. It is synthesized as high molecular weight and is degraded very fast by hyaluronidase enzymes or reactive oxygen species with the formation of fragments having decreasing sizes [24,25]. The biological effects of hyaluronate depend heavily on its molecular weight. In the first phase of the healing process, high molecular weight hyaluronate modulates inflammatory cells and fibroblast cell migration and promotes access at the wound site of polymorphonuclear leukocytes. Successively, low molecular weight hyaluronate promotes leukocyte chemotaxis and induces cytokine response [26,27].

In this study, either high molecular weight or low molecular weight sodium hyaluronate was loaded into *in situ* gelling carbohydrate powders with the aim of investigating hyaluronate impact on the technological properties of a complex polysaccharide blend alginate-pectin-chitosan and the possible synergies between polymers in the wound healing process. Hence, size distribution, morphology, fluid uptake ability, rheology properties, thermal analysis, and FT-IR spectra of the *in situ* gelling powders were thoroughly examined. Furthermore, to estimate the efficacy of the powders the *in vivo* wound healing assay using an excision murine model, was performed.

2. Material and methods

Sodium hyaluronate, from *Streptococcus equi,* high molecular weight (1500–1800 kDa) was purchased by Sigma Aldrich (Milan, Italy), while sodium hyaluronate low molecular weight (184 kDa) was kindly donated by Altergon (Avellino, Italy). Chitosan low molecular weight (50–190 kDa, 1 % viscosity in acetic acid 20–80 mPa s; 75–85 % deacetylated) was obtained by Sigma Aldrich (Milan, Italy). Sodium alginate from brown algae (1 % viscosity 35 mPa s; medium molecular weight 180 kDa, mannuronic/guluronic ratio 70/30) was given by Dompè S.p.A (L'Aquila, Italy), whereas pectin amid *CF* 025 D (amidated low methoxy grade, degree of esterification 23–28 %, degree of amidation 22–25 %, molecular weight 120 kDa) was kindly donated by Herbstreith&Fox (Werder/Havel, Germany). Acetic acid used for the dissolution medium, sodium chloride and ketamine hydrochloride/xylazine hydrochloride solution were obtained from Sigma-Aldrich, (Milan, Italy). Potassium dihydrogen phosphate buffer was acquired from VWR International (Milan, Italy). Mycological peptone was purchased from Oxoid Ltd., Basingstoke, Hants, United Kingdom) and fetal bovine serum qualified, heat inactivated from Gibco (Thermo Fischer Scientific, Brazil). All other chemicals used in this work were of commercial analytical grade.

2.1. Alginate, pectin, chitosan, and hyaluronate-loaded powders production

Powders composed of alginate, pectin, and chitosan were produced by mini spray drying setting the total polymers concentration at 0.15 % (*w/V*). Different ratios of alginate-pectin-chitosan (1:1:1, 1:1:3, and 1:1:7) and various sodium hyaluronate concentrations (0.5, 1.00, and 2.00 % *w*/w) were investigated. Feed solutions for spray drying were obtained as follows:

- Chitosan solution (C) was prepared by dissolving the polymer in an acid aqueous solution (1 % w/w CH_3COOH) at room temperature, under a gentle stirrer overnight;
- Alginate and pectin solution (AP) was prepared through initial solubilization of the alginate followed, after its dissolution, by the addition of pectin, at room temperature under a vigorous stirrer;
- After that, the two solutions were joined flush and homogenized through the use of Ultra-Turrax® T25 (IKAWorks GmbH & Co. Staufen, Germany) thus obtaining the final solution (APC solution);
- Finally sodium hyaluronate (H) was added to an APC solution under gentle stirring to obtain APCH.

All feed solutions were processed by Mini Spray Dryer B-290 (BuchiLaboratoriums-Tecnik, Flawil, Switzerland) with the optimized parameters reported in the table below:

Particles obtained were characterized in terms of process yield calculated as the ratio between the amount of product obtained and the total amount of the material processed.

2.2. Morphology and particle size distribution

The morphology of all powders was observed by scanning electron microscopy (SEM), using a Tescan Solaris instrument (Tescan Orsay Holding, Czech Republic). To verify the uniformity of the particles no <20 SEM images were taken. Powders were dispersed on an aluminum stub (Agar Scientific, Stansted, UK) and were coated with a thick gold layer (200–400 Å) (LEICA EMSCD005 metallizator) before microscopy.

Particle size distribution was evaluated both with SEM analysis and with static light scattering (LS) (N5, Beckman Coulter, Miami, Florida), making the average of three measurements for each sample. Each formulation was diluted in dichloromethane (DCM) and sonicated three times for 10 min: some drops of each formulation were placed into the cell to obtain an obscuration between 8 % and 12 %. Results, calculated by instrument software using the Fraunhofer model, were expressed as mean diameter.

2.3. Hyaluronate content and encapsulation efficiency

Hyaluronate (H) content was calculated as the ratio between experimental H weight and powder weight while encapsulation efficiency (e.e.) was calculated as the ratio of experimental to theoretical H content as previously reported [28]. Briefly, about 3 mg of the different formulations was stirred in 10 mL of potassium dihydrogen phosphate buffer (0.05 M, pH 7.00) to obtain a uniform dispersion. This dispersion was shortly sonicated, and centrifuged (3000 rpm for 10 min) and the supernatant obtained was filtered (filters of 0.45 μm) and analyzed by HPLC following a method reported in the literature [29]. The Agilent 1260 Infinity instrument (Agilent Technologies, USA) with a DAD detector, set at 205 nm, was used for the HPLC analysis. The separation was performed on a size exclusion column (PolySep-GFC-P 6000, 300 × 7.8 mm, Phenomenex, USA) with a guard column (PolySep-GFC-P 35 × 7.8 mm) using as isocratic mobile phase a potassium dihydrogen phosphate buffer (0.05 M) with pH adjusted to 7.0 using potassium hydroxide (10 %), at room temperature. The flow rate was of 1 mL/min and the injection volume was 20 μL. The method was validated respecting linearity range (concentration range 0.6–0.03 mg/mL, R^2 =

0.9999 and 0.6–0.08 mg/mL, $R^2 = 0.9997$) for H low molecular weight and high, respectively.

2.4. Fluid uptake ability

Fluid uptake ability was carried out using the Franz diffusion cell. Briefly, the membrane disc filter (PES, 0.45 μm, 25 mm, Pall Corporation, USA), previously weighed, was placed on the vertical receptor compartment of the Franz cell, filled with simulated wound fluid (SWF). This fluid with a final pH of 7.3, thermostated at 37 °C, was composed of 50 % fetal calf serum (Sigma Aldrich, Milan, Italy) and 50 % maximum recovery diluent (Sigma Aldrich, Milan, Italy) consisting of 0.1 % (*w/v*) peptone, a peptic digest of animal tissue, and 0.9 % (w/v) sodium chloride [30,31]. About 8 mg of powder was placed on a membrane and at regular time intervals, the swollen powders were removed and weighed. The degree of fluid uptake was determined as the ratio between the weight of the swollen sample at specific time intervals and the weight of the dried. All experiments were performed at least in triplicate.

2.5. Rheological studies

The rheological properties of *in situ* gelling powders were evaluated following a modified protocol present elsewhere [32] using an Anton Paar MCR-102 Rheometer fitted with plate-plate geometry (PP25 with a diameter of 24.985 mm) and the distance between the plates was set at 1 cm. Amplitude sweep tests were performed setting strain amplitude in the range 0.01–100 % with a constant angular frequency at $\omega = 10$ rad/s. All measurements were carried out at 37 °C. Each powder (150 mg) was placed directly on the plate, previously heated, and treated with SWF to form a gel. The results are reported in the form of a graph (loss and storage moduli *vs* shear strain), also analysing the loss factor behaviour (tan δ). Generally, in practical applications, $0.01 < \tan\delta < 1$ explains a gel-like behaviour, where 0.5 represents the transition point from a prevalent solid-like to a prevalent liquid behaviour.

2.6. Adhesion strength measurement

The adhesive properties of the *in situ* formed hydrogels were assessed using a modified protocol of the ASTM D3808 standard with a tensile stress tester, specifically the Electroforce 3200 testing instrument (Bose, Eden Prairie, MN), following procedures detailed elsewhere [17]. Briefly, was applied onto a nitrocellulose membrane filter (with a pore size of 0.45 μm and an area of 3.14 cm^2) that had been pre-conditioned with SWF. After the gel had formed as a result of contact between the formulation and the fluid, the membrane was positioned on the movable horizontal sample holder of the apparatus. The sample holder was then moved at a constant rate of 1 mm/min, leading to the compression of the gel against the measuring head of a calibrated load cell. The force-time curve generated during this process was recorded on a personal computer and, using LabChart 8 (AdInstruments, Oxford, UK), the force at which the gel detached from the substrate was calculated. All experiments were performed at least in triplicate.

2.7. Differential scanning calorimetry

Differential Scanning Calorimetry (DSC) (Mettler Toledo DSC 822e module controlled by Mettler Star E software, Columbus, Ohio) was used to determine the thermal characteristics of raw materials and formulations. 5–6 mg of the powder sample was weighed with a microbalance (MTS Mettler Toledo, OH, USA) before being placed in an aluminum pan (40 μL) perforated. Samples, so prepared, were heated from 25 °C to 400 °C at a rate of 25 °C/min and the characteristic peaks were recorded.

All DSC analysis was performed in a nitrogen atmosphere of 150 mL/min.

2.8. Fourier transform infrared spectroscopy

The different produced powders were subjected to solid state FT-IR characterization in the range of 4000–600 cm^{-1} using Spotlight 400 N (FT-NIR Imaging System, Perkin Elmer Inc., USA) equipped with a MIRacle ATR accessory with ZnSe crystal plate. The spectra were obtained at a resolution of 2.0 cm^{-1} using 128 scans. To better identify differences between samples a more accurate analysis was performed in a range from 1800 to 1200 cm^{-1} increasing the number of scans to 254. The results were evaluated using different spectrum function of the software Spectrum. Concerning the detailed analysis, a mathematical difference of normalized APC spectrum from normalized APCH spectrum was reported (to normalize spectra, an auto calculation of the factor to obtain the least square difference spectrum was used).

2.9. In vivo wound healing assay

All experiments involving animals were ethically and scientifically approved by the institute and the National Animal Laboratory ethics committee (National Husbandry accreditation 483/17.12.2019; specific experiments for the presented study approved by National Laboratory Regulatory bodies). One significant challenge using animal models to evaluate wound repair is that wound contraction originates outside of tissue, whereas in humans, processes as re-epithelialization and granulation tissue formation occurs within the wound space, therefore we used two approaches in our experiments, one that uses silicone ring to evaluate re-epithelialization and granulation tissue formation and the other to keep the naturally healing processes, namely wound contraction. 8 weeks old 12 mice of strain C57Black/6/group (sex ratio 1:1) were employed in the *in vivo* wound healing experiments. Mice were individually weighed (18–26 g) and after the procedure single housed in standard open cages with free access to food and water. The mice were anesthetized with a ketamine/xylazine mixture (100 mg/10 mg/kg) administered intraperitoneally. Hair was removed from the dorsal, interscapular zone with a trimmer, and after depilatory cream was applied. The mouse was placed on a heated plate and the skin was decontaminated with 70 % ethanol and betadine. To compensate for fluid loss 1 mL saline was given subcutaneously and for pain management, 3 doses of meloxicam (3 mg/kg), one every 24 h were administered subcutaneously.

All mice were randomly divided into two experimental groups: wound kept open by ring group and naturally healing group. In the first group hyaluronate-loaded formulation was compared to marketed wound healing cream Ialuset®. In the second group hyaluronate-loaded formulation was analyzed in comparison with cream Ialuset® and normal healing. On each mouse, two wounds of 5 mm were made with a biopsy punch and sterile silicon splints were placed over the wound and secured to the skin with tissue glue and four points of suture (6.0 nylon). The detailed procedure of the excisional animal model was first published in 2012 by Ren et al. and further elaborated by Zomera al [33,34]. In all groups, powders (20 mg for the *in situ* gelling powders without gauzes or cream) and cream were applied at day 0, without any other re-application. In controls, only at day 0 an antibiotic was applied to avoid infection. After the sample application, every single mouse was placed on a heated pad for recovery and then placed back in the cage where wet food was added. After that, normal healing was followed for any infection and/or inflammation. Since no complications were registered in the groups, other antibiotics and/or anti-inflammatory procedures were avoided and the wound area was recorded for 10 days. On day 10, 50 % of mice, were sacrificed with a high dose of an anesthetic mixture, and skin samples were harvested for histology. The wound areas were analyzed by Image-J software and the wound closure percentage was calculated by the formula, as follows:

$$Wc = \frac{A_0 - A_t}{A_0} \times 100$$

where A_0 and A_t are the wound area at day 0 and at time point t, respectively.

An overall scheme of the murine model used to test the wound healing dynamics is reported in Fig. S1.

2.10. Histological analysis and immunohistochemistry

The skin samples were stored in labelled tubes with a fixative at 4 °C. The samples were individually fixed in 10 % buffered formaldehyde for 24 h. After the fixing period, the tissue fragments were subjected to the following processes: washing, dehydration, clarification, paraffination, and inclusion in paraffin. Briefly, for the histopathological processing by automatic tissue processor Microm STP 420D, the following steps were done: washing with running water for 1.5 h; dehydration in ethyl alcohol using 3 baths: 70° (for 90 min), 80° (for 105 min), 96° (for 105 min) at 37 °C; dehydration in absolute ethyl alcohol using 3 baths left to act for 4 h at a temperature of 37 °C; clarification in xylene using 3 baths for 6 h at a temperature of 52 °C; paraffining in 4 bathrooms for 6 h at the temperature of 58 °C. After inclusion in the paraffin, the tissue fragments were cut to the size of 3 μm using automatic rotating microtomes type Leica RM 2265. Subsequently, the tissue sections were displayed on simple blades for the usual staining (Hematoxylin Eosine-HE) on slides. After deparaffination of the slides and hydrating with ethyl alcohol, the procedure was as follows: wash the glass slides with running water; colour the slides with hematoxylin; leave for 30 s to 5 min; wash with tap water; treat with alcohol-hydrochloric acid; wash the blades with tap water; contrast the slides in water for 10 min, colour the slides with eosin for 10–15 s dehydrate the slides; clarify and mount using the Leica CV 5030 automatic mounting device.

2.11. Statistical analysis

Data are reported as mean ± standard deviation (SD) of at least three independent experiments, each in triplicate. Analysis of variance and Bonferroni's test were used for data analysis to perform multiple comparisons, using Graph Pad Prism 8 (GraphPad Software). A P value <0.05 was considered significant.

3. Results and discussion

3.1. Powders preparation

Several polymeric blends composed of alginate, pectin, and chitosan with different ratios have been used to produce spray-dried powders (APC) loaded with two molecular weights sodium hyaluronate (H) in order to assess their feasibility of performing as *in situ* forming wound dressing. High M content alginate was used to stimulate cytokine production by human monocytes, while amidated pectin was chosen to increase the *in situ* gel rate both to enhance the antibacterial properties and healing stimulation of chitosan. Based on previous work [23], spray drying feed concentration was set at 0.15 % (*w/v*), while different polymer ratios, namely APC 111, 113, and 117 were used to produce powders (see Table 1). Starting from the formulation containing the lowest amount of chitosan, APC 111, sequential increases in quantities of H were implemented within the polymer blend. His investigation encompassed the exploration of the influence of two distinct molecular weights, high molecular weight (HH) and low molecular weight (LH) hyaluronate on the resultant powders, denoted as APCHs 111. Encouraged by promising outcomes in terms of powder yield and properties, the scope of the study extended to the formulation with elevated chitosan content: APCH 113 and APCH 117.

The spray drying atomization process led to good yields for all powder formulations, demonstrating the possibility of producing powder from feeds in the form of micro dispersed suspensions, as in the case of feed with high chitosan content. Notably, the yield exhibited a direct correlation with chitosan concentration; higher chitosan levels corresponded to elevated yields, culminating in approximately 70 % yields for APC 113 and APC 117. Moreover, the increase in H amount in APCH 111 led to a higher yield, moving from 56 to 68 %, and encapsulation efficiency (e.e.) of about 100 %, regardless of H molecular weight (Table 1). These results are in line with literature data reporting that the process yield, as well as e.e., is directly proportional to the feed solution concentration. High polymer concentration means a higher amount of polymer in the atomized droplets with the formation of larger particles easier to collect [35]. In the same way, as explained by Mishra et al., since the rate of solvent evaporation controls the deposition of solute at the surface of the drying droplet, higher polymeric concentration results in better encapsulation [36].

Feeds formulated with elevated chitosan and hyaluronate content exhibited the development of flocculates, attributed to the creation of a polyelectrolyte complex between hyaluronate and chitosan [37,38]. This complex formation posed challenges to the atomization process, presenting some difficulties in powder production, except APCH 113–0.5H and APCH 113–0.5H, whereas in the case of APCH 117-2H feeds were unprocessable, due to the extent of flocculation in the feed (Table 2).

3.2. Particle size and morphology

APC and APCH formulations exhibited different sizes, as reported in Table 1. The presence of chitosan exerted a notable influence on this powder properties, with smaller particles obtained when chitosan concentration in the feed was increased. In fact, during the spray drying process, the intrinsic viscosity of chitosan within feeds (APC 113, APC 117, APCH 113, APCH 117) hindered the diffusion of alginate and pectin within the drying droplets. This restricted diffusion resulted in the formation of more densely packed and uniform particles [39]. Concerning size associated with the different formulations, it is evident a discrepancy emerged between the size of the microparticles investigated by LS and SEM-based image analyses. Probably liquid-based LS analysis was affected by aggregation phenomena due to the inability of the liquid to discharge powder surface charges resulting in an apparent larger size distribution compared to the analyses obtained by SEM images [40].

Furthermore, SEM images in Fig. 1 show that the particles containing increasing amounts of chitosan displayed higher surface roughness, pores, and clusters. This difference in particle morphology can be related to the increase in the alginate-chitosan ratio, leading to a greater formation of polyanion-polycation complexes within the feed, and consequently to aggregates and structural irregularities in the solid particles [41,42]. On the contrary, neither the presence nor the amount of H leads to any discernible influence in the morphology of the resulting particles, therefore in Fig. 1 were reported only the particles loaded with LH.

3.3. Characterization of the in situ gelling powders

To evaluate the fluid uptake ability, a key feature for *in situ* gelling powders to control both the gelling rate when in contact with wound fluids and the release of encapsulated biomolecules, an extensive investigation was conducted through fluid absorption experiments using

Table 1
Parameter of the mini spray drying.

Inlet Temperature (°C)	Outlet Temperature (°C)	Aspirator (%)	Air pressure (atm)	Drying air flow (L/h)	Feed rate (mL/min)	Nozzle diameter (mm)
120	65–68	100	6	560–580	5	0.5

Table 2
Composition, process yield, particle size, drug content, and encapsulation efficiency (e.e.) of powders obtained with different polysaccharides ratio by mini spray drying.

Sample	Hyaluronate concentration % (*w/w*)	Yield (%)	Hyaluronate content (%) ± SD	e.e. (%) ± SD	Mean diameter (μm) ± SD[a]	Mean diameter (μm) ± SD[b]
APC 111	–	60	–	–	3.82 ± 0.12	6.24 ± 0.13
APC 113	–	72	–	–	2.55 ± 0.09	2.55 ± 0.10
APC 117	–	73	–	–	2.28 ± 0.05	2.58 ± 0.04
APCH 111-0.5HH	0.5	56	0.37 ± 0.04	73.98 ± 6.87	3.64 ± 0.08	6.43 ± 0.02
APCH 111-1HH	1.0	59	0.97 ± 0.03	98.76 ± 3.12	3.11 ± 0.07	9.00 ± 0.04
APCH 111-2HH	2.0	66	1.98 ± 0.03	99.99 ± 1.50	3.45 ± 0.09	12.55 ± 0.01
APCH 113-0.5HH	0.5	72	0.41 ± 0.02	85.15 ± 4.13	2.79 ± 0.04	3.19 ± 0.04
APCH 117-0.5HH	0.5	71	0.40 ± 0.02	80.58 ± 2.82	2.45 ± 0.01	3.55 ± 0.01
APCH 111-0.5LH	0.5	57	0.45 ± 0.03	90.13 ± 5.73	3.31 ± 0.09	9.11 ± 0.20
APCH 111-1LH	1.0	58	1.00 ± 0.01	99.98 ± 2.00	3.19 ± 0.07	12.61 ± 0.06
APCH 111-2LH	2.0	68	2.00 ± 0.02	99.99 ± 1.24	3.44 ± 0.13	13.95 ± 0.23
APCH 113-0.5LH	0.5	69	0.41 ± 0.03	85.85 ± 5.07	2.83 ± 0.06	2.95 ± 0.02
APCH 117-0.5LH	0.5	70	0.39 ± 0.01	78.42 ± 2.04	2.72 ± 0.08	3.50 ± 0.06

[a] Mean diameter from SEM images.
[b] Mean diameter from LS analysis.

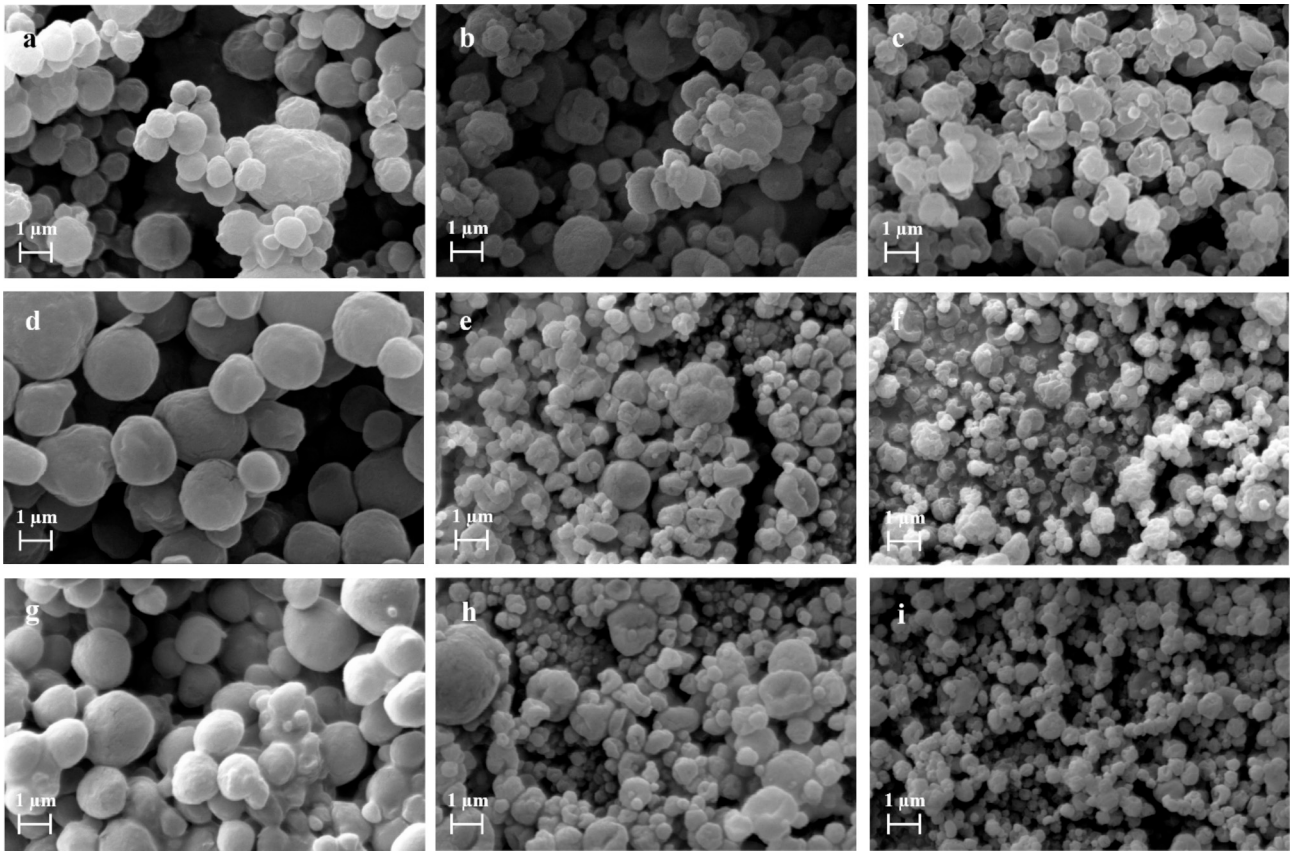

Fig. 1. SEM microphotographs of *in situ* gelling powders. Blank particles made by alginate-pectin-chitosan at different ratios: (a) APC 111, (b) APC 113, (c) APC 117; second line particles with high molecular weight hyaluronate (d) APCH 111–0.5HH, (e) APCH 113–0.5HH, (f) APCH 117–0.5HH; third line particles with low molecular weight hyaluronate: (g) APCH 111–0.5LH, (h) APCH 113–0.5LH, (i) APCH 117–0.5LH.

a simulated wound fluid (SWF). As shown in Fig. 2 all APCH formulations reached their maximum swelling in about 5–15 min, followed by an equilibrium phase extending throughout the experimental duration. APCH 117 showed a faster uptake despite being the powder that needed a longer time to reach its peak in fluid uptake. This phenomenon can be explained considering that powders with higher amounts of chitosan which concurrently featured particles with smaller size and a wrinkled surface were able to enhance the surface contact area between the particles and the SWF, consequently fostering higher fluid absorption levels. Moreover, it is interesting to highlight that the formulations

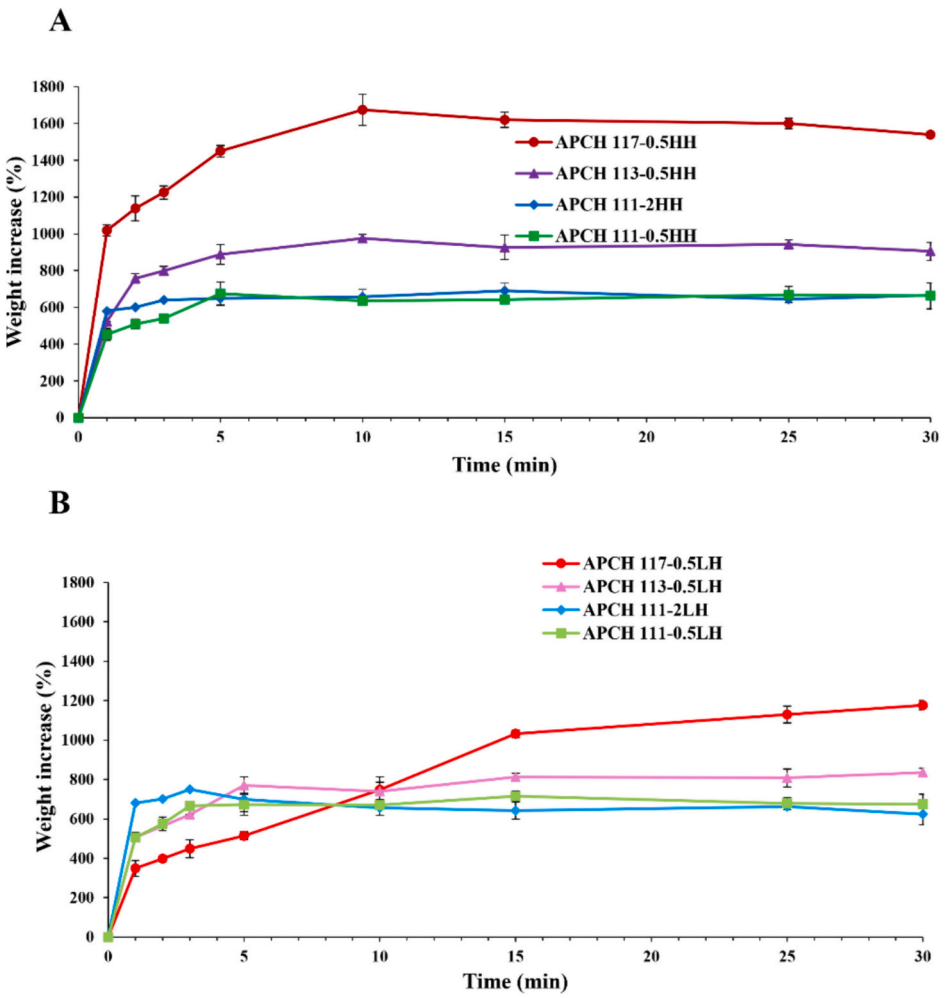

Fig. 2. Simulated wound fluid uptake of different APCH formulations. Panel A: APCHs loaded with high molecular weight hyaluronate; Panel B: APCHs loaded with low molecular weight hyaluronate.

loaded with LH showed lower uptake compared to formulations containing HH. This disparity was most pronounced in formulations featuring increased chitosan concentrations, namely APCH 113, and APCH 117, due to the formation of polyelectrolyte complexes between positively charged chitosan and negatively charged sodium hyaluronate [43]. The difference in the medium uptake could be related to the difference in the length of hyaluronate chains [44]. In fact, longer chain polymer (HH) is characterized by lower mobility and thus reduced possibility of forming polyelectrolyte complexes. On the other hand, short chain polymer (LH) showed higher flexibility, thus higher complexation ability with chitosan resulting in a slower uptake rate [45]. On the contrary, the amount of H added to the formulation, whether 0.5 % or 2.0 %, did not affect the ability of the powders to absorb the fluid.

To assess the impact of loading either HH or LH on the properties of the *in situ* formed gel both adhesive and comprehensive rheological studies were conducted. Specifically, adhesive strength analyses of the *in situ* formed hydrogel were evaluated using a modified protocol of ASTM D3808 standard, using SWF conditioned nitrocellulose membrane filter as adhesion substrate. Adhesive strength for the formulations was in the range of 7.8–9.7 kPa. Higher adhesiveness was exhibited by hydrogels containing HH and higher amounts of chitosan, with the increase of chitosan being predominant in such effect due to the formation of highly entangled and polymer chain interaction during the fluid uptake. Nevertheless, such a range in adhesiveness can allow easy and atraumatic removal of the gel from the wound bed after use, while minimizing its accidental removal after administration [46].

Starting from the adhesiveness results related to formulation loaded with different molecular weight H, to better understand the differences in the gelation behaviour, rheological investigation was carried out. Thus, oscillatory test was performed to elucidate the structural integrity of the *in situ* formed gels. Macroscopically, as reported in Fig. 3B, all samples showed a viscoelastic behaviour described by the dominance of storage modulus (G'), a key indicator of gel elasticity. The incorporation of HH led to a minimal influence on the consistency of the hydrogels, as confirmed by a comparable value of loss factor at rest (0.24 for APC 111 and 0.25 for APCH 111–2HH). On the contrary, the loading of LH led to a decrease in loss factor (0.18), highlighting a rigid consistency in the resulting gel structure. This difference in gelation between powders loaded with HH or LH can be attributed to the different mobility of polymer chains (higher molecular weight means lower mobility), thus the increased ability of LH to interact with other carbohydrates could explain the difference in the final consistency of gels [47]. Such results could explain the differences in the hydrogel adhesiveness between HH and LH loaded formulations confirming that hydrogels containing HH might be more adhesive compared to those containing LH.

To investigate the impact of H on the physicochemical properties of APC powders, an analysis of their thermal behaviour was conducted through DSC. As reported in Fig. 4-panel A, all polymers in the form of raw material exhibited a large endothermic band from 90 to 145 °C indicative of the presence of bound water. Among the single components, alginate (Fig. 4A-b) presented an exothermic peak around 240 °C

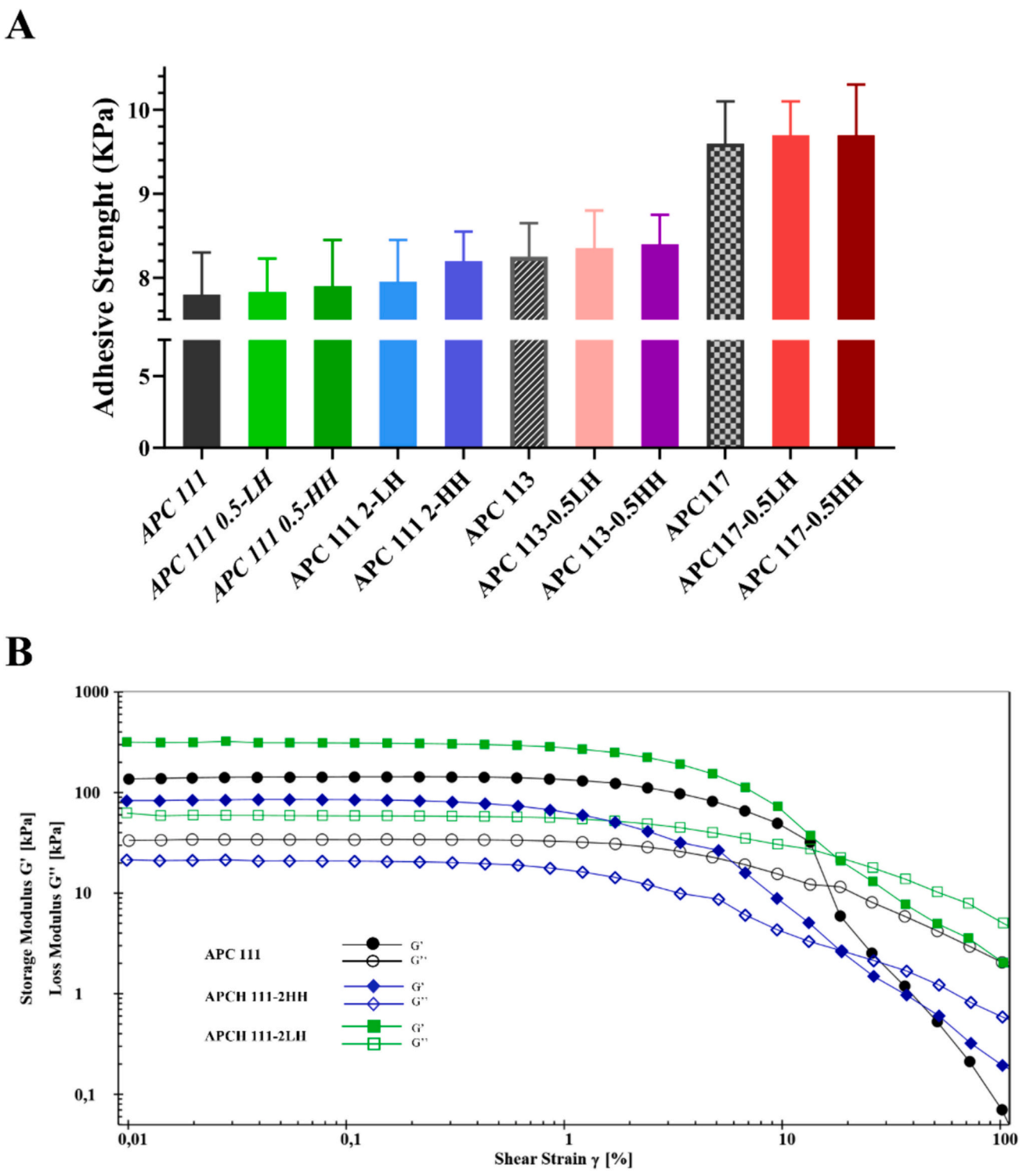

Fig. 3. Panel A: Adhesive strength of hydrogels obtained by APCs loaded with different amount and hyaluronate in comparison with the unloaded powders. Panel B: Amplitude sweep test of *in situ* gelled powders, storage modulus (G′), and loss modulus (G″) of APC 111 (green) in comparison with APCH 111–2HH (blue) and APCH 111–2LH (green). (For interpretation of the references to colour in this figure legend, the reader is referred to the web version of this article.)

related to its oxidative degradation [48], while amidated pectin (Fig. 4A-a) showed an endothermic peak at 145 °C related to its melting point [49], a broad peak at 190 °C followed by an exothermic peak at 250 °C due to polymer oxidative degradation, while chitosan (Fig. 4A-c) exhibited a broad peak around 300 °C related to its degradation [50]. H (Fig. 4-d,e) contains three types of functional groups capable of hydrogen bonding with water: hydroxyl, carboxylic, and acetamide groups that have been responsible for the endotherm peak related to the removal of water, up to 200 °C. Moreover, an exothermic peak at 238 °C is related to its thermal decomposition [51]. The differences in the thermal behaviour of H due to the different molecular weights were highlighted through the evaluation of glass transition (HH glass transition temperature 182.78 °C, while LH glass transition temperature 168.73). In fact, polymers with higher molecular weight are

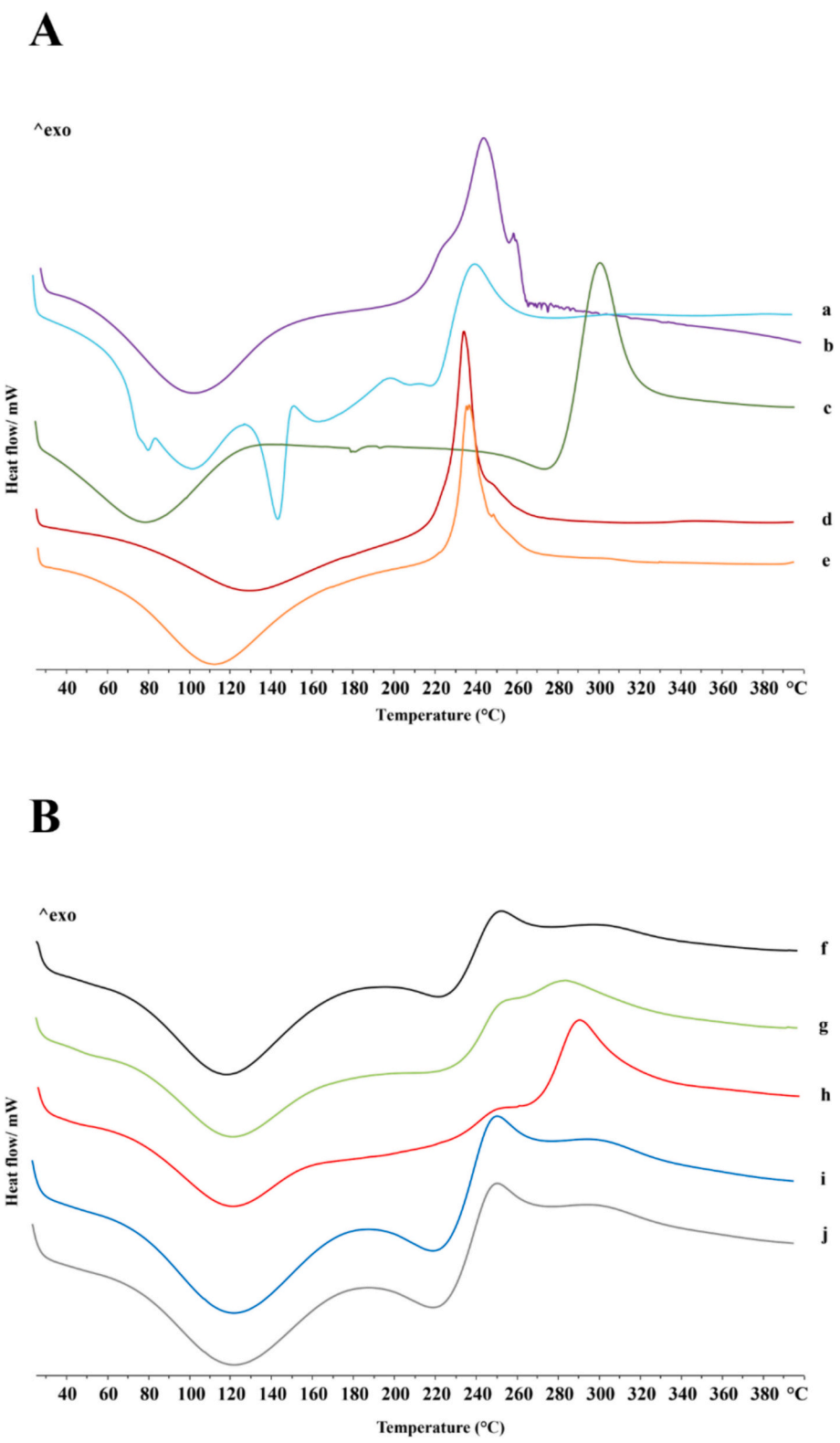

Fig. 4. Differential scanning calorimetry thermograms of alginate, amidated pectin, chitosan, and sodium hyaluronate raw material in comparison to *in situ* gelling powders. Panel A: amidated pectin (a), alginate (b), chitosan (c), sodium hyaluronate high molecular weight (d), sodium hyaluronate low molecular weight (e). Panel B: APC 111 (f), APC 113 (g), APC 117 (h), APCH 111-2HH (i) and APCH 111-2LH (j)

characterized by longer chain with reduced mobility and thus more energy is required for the glass transition [52].

In Fig. 4-panel B is reported a comparative analysis between the calorimetric thermograms of blank formulations and those containing H. Blank formulations APC 111, APC 113, and APC 117 exhibit distinct thermal profiles (Fig. 4B-f, g, h). Particularly, formulations with higher chitosan content, such as APC 113 and APC 117, demonstrate an initial broad peak at 120 °C, signifying the presence of water (both surface-bound and crystallization). This peak is shifted to higher temperatures compared to APC 111, probably due to a more robust immobilization of

water molecules amidst chitosan chains, as supported by prior research [41]. Furthermore, APC formulations exhibited a structural rearrangement at 250 °C followed by a broad peak around 300 °C related to chitosan degradation. In the case of APC 111, an exothermic peak at 250 °C is associated with alginate and pectin, while another peak near 300 °C is correlated to chitosan degradation (Fig. 4B-f). APC 117, on the contrary, exhibited an opposite trend due to its higher concentration of chitosan. In fact, the initial peak is broadened compared to the peak at 290 °C, indicative of the formation of a polyelectrolyte structure between the carboxylate group of the alginate and ammonium group of chitosan (Fig. 4B-h). The high amount of chitosan contributes to the creation of a protective layer around the polyelectrolyte structure, enhancing its thermal resistance and leading to degradation at elevated temperatures [41]. The calorimetric profile of APCH 111–2HH mirrored that of APCH 111–2LH, with the hyaluronate-related peak difficult to distinguish (Fig. 4B-i,j). Specifically, a single peak at 249 °C linked to the exothermic rearrangement of alginate, pectin, and H was observed. The effect of different H chain lengths, observed in the glass transition of raw material, could be also observed in the hyaluronate-loaded powders focusing the attention on both endothermic and exothermic peaks previously mentioned that are slightly shifted at higher values for particles with HH. From a macroscopic point of view, hyaluronate-loaded powders showed the same thermal behaviour as APC 111. This phenomenon endorses the formation of a homogeneous blend between the polymers through the formation of a polyelectrolyte complex [53].

The interaction between H and APC matrix was finally elucidated

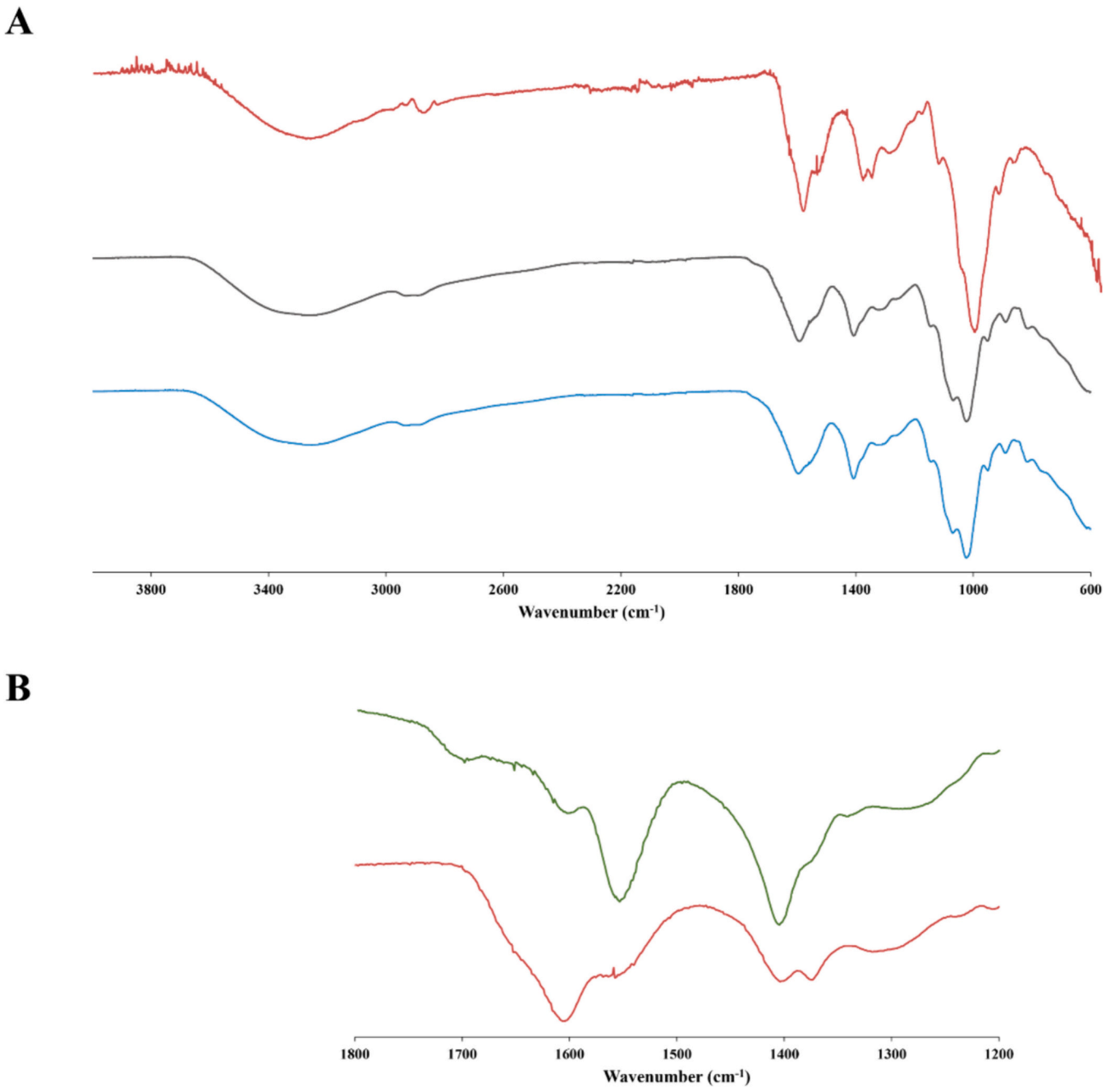

Fig. 5. Panel A: FT-IR spectra of sodium hyaluronate in comparison to blank and loaded with sodium hyaluronate: sodium hyaluronate raw material (red), APC 111 (black), and APCH 111-2HH (blue). Panel B: Spectra in the wavelength range from 1800 to 1200 cm^{-1} of sodium hyaluronate (red) and mathematical difference between normalized APC and APCH 111–2HH spectra (green). (For interpretation of the references to colour in this figure legend, the reader is referred to the web version of this article.)

through FT-IR analysis. Fig. 5A shows the complete spectra of H raw material, APC 111, and APCH 111–2H. H spectrum exhibited a broad band spanning from 3100 to 3400 cm^{-1} related to the NH and OH stretching, accompanied by a less intense band around 2800 cm^{-1} attributed to the CH stretching. Moreover, a dual peak at 1602 and 1551 cm^{-1} facilitated the identification of characteristic acetylamide groups (-NH·CO·CH_3), while the other two peaks at 1404 and 1373 cm^{-1} can be ascribed to the methyl group deformation, with a pronounced band linked to C-O-C stretching at approximately 1027 cm^{-1} [54]. On the other hand, the APC 111 spectrum exhibited the most representative peaks of alginate, pectin, and chitosan such as at 1592 cm^{-1} the COO^- vibration of alginate, the pectin peaks of $CONH_2$ and $COCH_3$ at 1400 and 1724 cm^{-1}, and the chitosan NH_3 deformation at 891 cm^{-1} [55]. APCH 111-2H spectrum it was possible to detect almost all peaks previously mentioned. However, due to the structural similarity among each component of APCH 111-2H, the reliability of direct comparison was limited. Consequently, a meticulous FT-IR mathematical assessment was conducted in the range of 1200 to 1800 cm^{-1} to ascertain the interaction of H within the polymeric matrix. Fig. 5B illustrates the spectrum derived from subtracting the normalized APC 111 spectrum from the normalized APCH 111-2H spectrum, and this spectrum was juxtaposed with that of raw H. Starting within the lower range around 1350–1400 cm^{-1}, the spectrum shows the merge of methylic group deformation peaks of H. Remarkable differences are observed in the wavenumber range from 1500 to 1800 cm^{-1}. In fact, in the spectrum obtained through the mathematical difference between normalized APC and APCH 111-2HH spectra, it is possible to observe two peaks at 1555 cm^{-1} and 1704 cm^{-1} that could be assignable to hyaluronate-chitosan interaction, *i.e.*, NH_3^+ from the chitosan and the COO^- of hyaluronate, respectively. Through this analysis, it becomes evident that the incorporation of H did not disrupt the matrix structure; however, H plays an active role in fostering polyelectrolyte complex formation with ammino groups [45,53]. No substantial distinctions were discerned between formulations loaded with different amounts of H, mirroring the trends observed in different polymer ratios [54].

3.4. *In vivo test on the promotion of wound healing*

Numerous studies have highlighted the possibility of using alginate or chitosan as accelerators of wound healing, exerting beneficial effects across different phases of the wound healing process [56,57]. These findings prompted an exploration into the potential of the *in situ* gelling powders to facilitate healing in mouse full-thickness skin defects. In preliminary studies conducted using a single application of APC 111, it was observed a substantial acceleration in wound closure over 7 days that outperformed normal healing processes (Fig. 6A). Upon application, the particles formed a soft hydrogel film that enveloped the entire wound site, without any visible macroscopic inflammatory responses or signs of infection over all the experiment duration. APC 111 exhibited a significant reduction in wound size compared to the control, indicative of the formulation potential effectiveness in minimizing wound dimensions.

In order to evaluate the potentiality of the hyaluronate-loaded powders to facilitate the healing process, a formulation with a high content of H was administered to the wound site in an *in vivo* assay. Since HH is noted for its superior performance in promoting wound closure compared to LH [58], and, no significantly relevant technological properties were observed between the formations loaded with different molecular weight H, wound closure evaluation studies were conducted using APCH 111-2HH.

Two distinct murine models were employed: one involving a silicon ring and the other keep the naturally processes. Representative photographs in Fig. 6B illustrate the macroscopic alterations at the wound site in the group that keep the naturally processes, with daily measurements of wound healing using a caliper. All mice were individually housed to verify any potential infection following the topical application on day

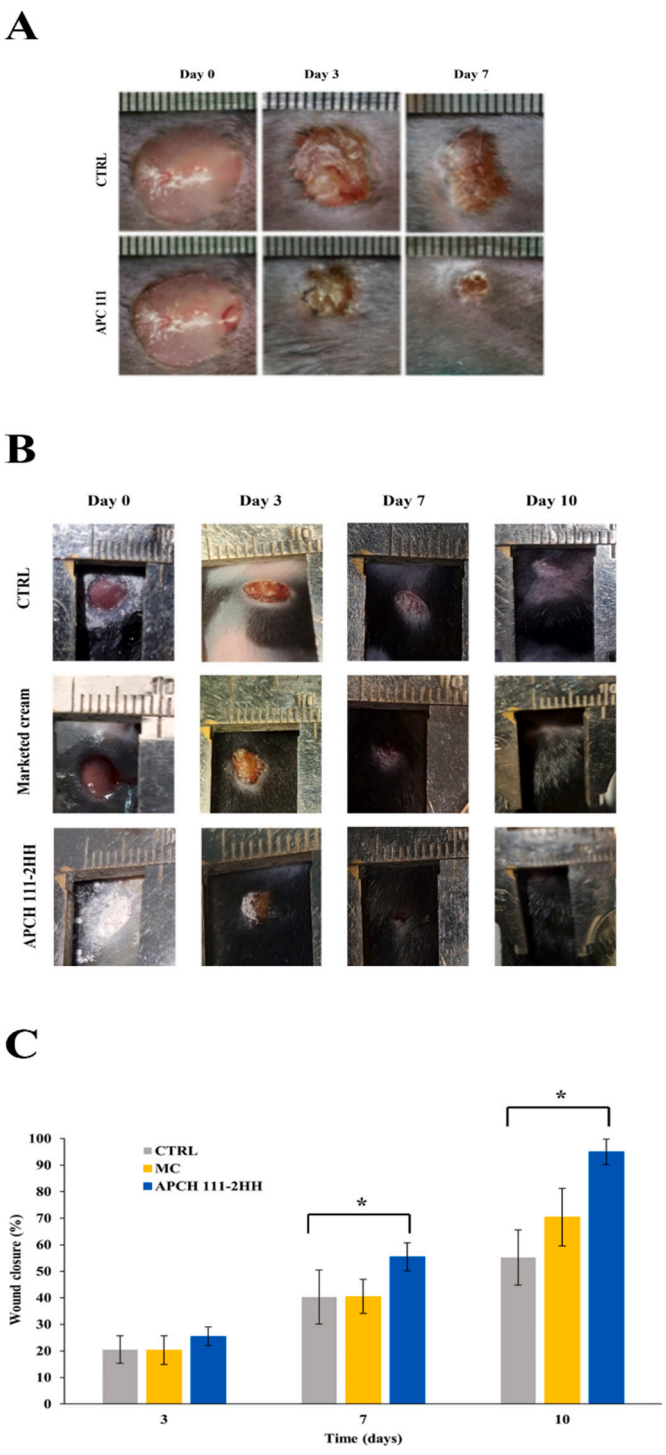

Fig. 6. *In vivo* effects of *in situ* gelling powders on the wound healing of a murine model. Panel A: Representative photographs of wound spot at days 0, 3, and 7 taken after full-thickness skin excision, APC 111 *vs* normal healing control just with antibiotic application on day 0. Panel B: representative macroscopic registration of wound healing at different time intervals, APCH 111-2HH *vs* normal healing control just with antibiotic application on day 0 *vs* marketed wound healing cream; Panel C: normalized wound closure percentage dynamics in control, marketed wound healing cream, and APCH 111-2HH treated mice groups at day 3,7,10.

0 of APCH 111-2HH and a marketed wound healing cream containing the same dose of H. Throughout the first week post-wound initiation, the healing percentages for all groups of mice, whether male or female, exhibited statistically comparable behaviours, except the APCH 111-2HH treated group, which showed a slightly higher healing percentage. After seven days, it became evident that the mice treated with APCH 111-2HH exhibited a significantly ($p < 0.05$) higher wound closure percentage compared to the control group and the marketed cream group. The latter groups still displayed macroscopically visible wounds (Fig. 6C), whereas the APCH 111-2HH treated group achieved complete wound closure within ten days. Since alginate and chitosan have reported beneficial effects on wound repair, this result could be attributed to the synergic effect of the polymeric blend.

Values are shown as mean ± SD, * $p < 0.05$ *vs.* control group.

Histology and immunohistochemical analysis were performed on samples obtained by silicon ring attached mice model, according to the above-described methodology. These studies were conducted to better evaluate the effect of the *in situ* gelling powder on specific biological processes involved in wound healing.

In control mice group, the central region of the wound area displayed a non-continuous epidermis after 10 days. The visible epidermal portion exhibited thickening and a multilayered appearance. The dermis showed significant inflammatory infiltrates, with the presence of numerous small blood vessels. Moreover, in areas where the dermis thickened, collagen fibrils were oriented horizontally (Fig. 7a). Among mice treated with the marketed cream, the epidermis detached from the dermis across a substantial portion of the injured area. This epidermis appeared thickened, particularly in the region connected to the dermis, which also exhibited the formation of granulation tissue. In the central area, collagen fibrils were dispersed in various directions (Fig. 7b).

In the APCH 111-2HH treated mice groups, a distinct delineation of the excision/treatment site within the epidermis was absent after 10 days. The subepidermal dermis displayed normal characteristics, including intact hair follicles. Toward the deeper layers, the dermis exhibited thickening, accompanied by an inflammatory infiltrate. In some cases, in fact, even at day 10th some inflammatory infiltrates were recognized, still matching the proliferation phases where cells are populating the wound to continue the process Importantly, the collagen fibrils in this group demonstrated an almost normal appearance (Fig. 7c).

Regarding the treatment with blank formulation (APC 111), histology revealed that the excised area was still visible after 10 days. The

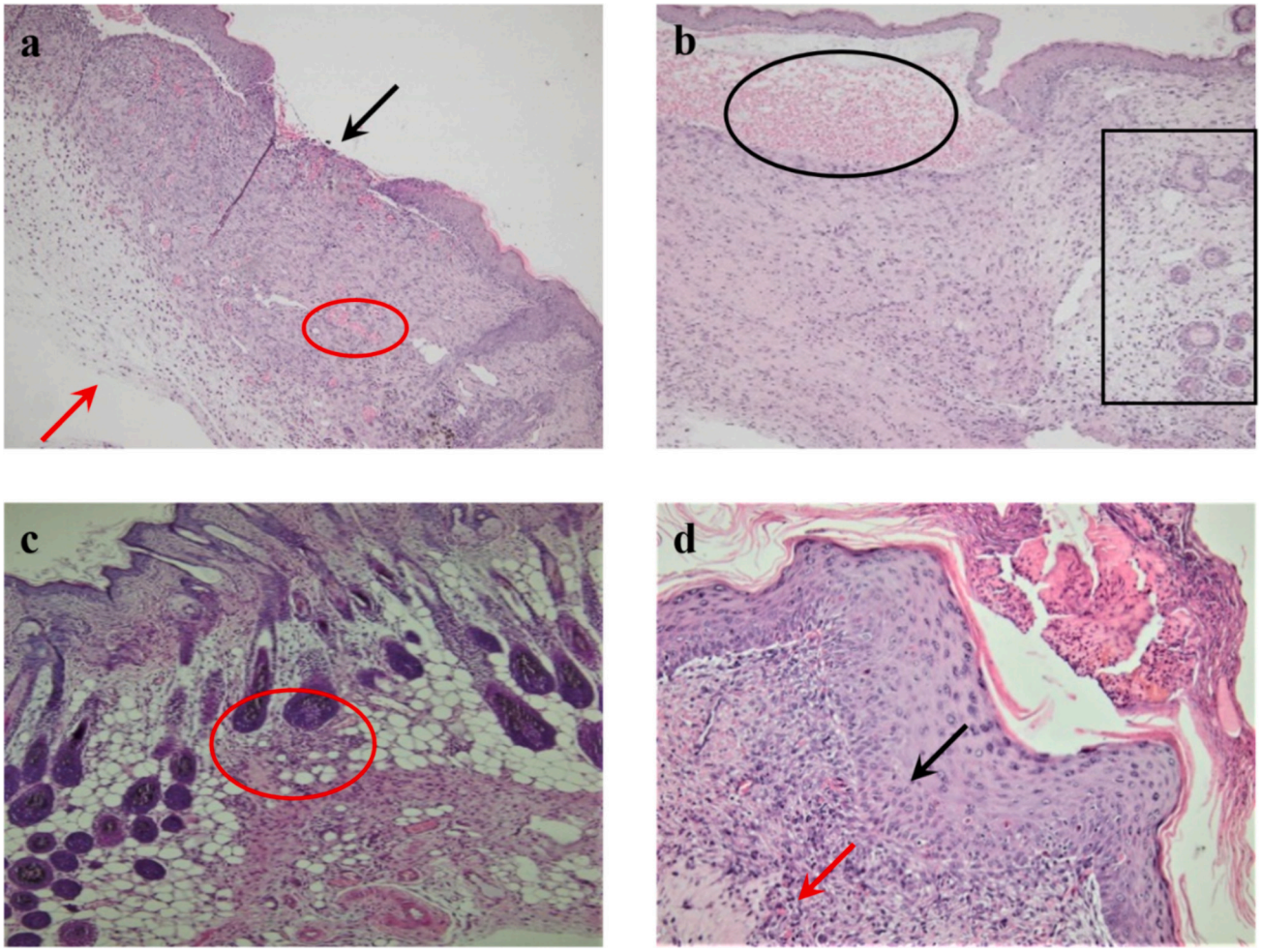

Fig. 7. Histological examples of wound healing in murine wound model where a silicon ring was used to avoid the lateral proliferation of the cell tissue: (a) no treatment, healed naturally; in the central region of the wound area a non-continuous epidermis is seen (black arrow), thick and a multilayered appearance; dermis with inflammatory infiltrates, and small blood vessels (red circle); horizontal collagen fibrils (red arrow) (H&E, Ob. 10×); (b) treatment with hyaluronic loaded marketed cream; epidermis detached from the dermis (black circle), thickened epidermis in contact to the dermis, granulation tissue (black square), collagen fibrils in various directions (H&E, Ob. 40×); (c) APCH 111-2HH treatment; subepidermal dermis is normal with intact hair follicles (red circle); thick dermis and inflammatory infiltrate; collagen fibrils normally organized (H&E, Ob. 40×); (d) APC 111 treatment; excised area present; thick epidermis (black arrow); enlarged dermis with inflammation, granulation tissue, and connective tissue expansion; no hair follicles and adjacent glands (red arrow) (H&E, Ob. 40×). (For interpretation of the references to colour in this figure legend, the reader is referred to the web version of this article.)

excised and treated area presented an epidermis thickened yet well-represented in the entire treated area. The dermis was enlarged, displaying signs of inflammation, granulation tissue, and connective tissue expansion. Consequently, hair follicles and adjacent glands were absent. Moreover, fibrous tissue and inflammation were observed on the epidermal surface (Fig. 7d).

Several studies have demonstrated the pivotal role of hyaluronic acid in wound healing and the advantages offered by the use of chitosan, including its ability to enhance hyaluronic acid deposition [26,53,58]. In our study, APCH 111-2HH demonstrated superior wound healing compared to the blank formulation and the marked hyaluronic loaded cream, indicating the ability to promote hyaluronic acid ability to contribute to inflammation, proliferation, and maturation stages, possibly through synergistic interactions with chitosan present in the powders.

4. Conclusions

Alginate-pectin-chitosan particles loaded with sodium hyaluronate have been effectively produced by spray drying technology. The polysaccharides blend was transformed into an *in-situ* gelling powder capable to quickly absorbing up to 15 times its weight in wound fluid. The *in situ* formed soft hydrogel demonstrated good elastic properties, enabling proper adhesion and retantion in the wound bed. DSC and FT-IR analyses demonstrated the interactions between carbohydrates and the consequent formation of polyelectrolyte complexes between polymers. Moreover, hyaluronate-loaded formulations exhibited enhanced wound healing properties in comparison with a marketed hyaluronic-loaded ointment in a skin excision model during a period of 10 days, promoting complete wound closure. Overall, these results suggest that hyaluronate-loaded *in situ* gelling powders promising candidates for the development of advanced wound dressing. The tailored formulation ability to conform to the wound bed, enhance wound closure, minimize inflammation, and promote tissue regeneration holds potential for clinical applications and therapeutic advancements in the treatment of chronic wounds.

Supplementary data to this article can be found online at https://doi.org/10.1016/j.ijbiomac.2024.133192.

CRediT authorship contribution statement

Chiara Amante: Writing – original draft, Investigation. **Monica Neagu:** Writing – original draft, Investigation. **Giovanni Falcone:** Visualization, Investigation. **Paola Russo:** Formal analysis, Data curation. **Rita P. Aquino:** Writing – review & editing, Validation. **Luigi Nicolais:** Writing – review & editing. **Pasquale Del Gaudio:** Supervision, Conceptualization.

Declaration of competing interest

Pasquale Del Gaudio reports financial support was provided by University of Salerno. If there are other authors, they declare that they have no known competing financial interests or personal relationships that could have appeared to influence the work reported in this paper.

Acknowledgement

Authors would like to thank Dr. Gheorghita Izvoranu, Head of Animal Husbandry, “Victor Babes” National Institute of Pathology, veterinary physician Dr. Laurentiu Anghelache, Dr. Emilia Manole, Dr. Mihaela Surcel, PhD student Adriana Munteanu and all the technicians within the Animal Husbandry for the thorough work done in developing the animal model of wound healing.

References

[1] F. Della Sala, G. Longobardo, A. Fabozzi, M. di Gennaro, A. Borzacchiello, Hyaluronic acid-based wound dressing with antimicrobial properties for wound healing application, Appl. Sci. 12 (6) (2022) 3091.
[2] S.R. Nussbaum, M.J. Carter, C.E. Fife, J. DaVanzo, R. Haught, M. Nusgart, D. Cartwright, An economic evaluation of the impact, cost, and Medicare policy implications of chronic nonhealing wounds, Value Health 21 (1) (2018) 27–32.
[3] R. Laurano, M. Boffito, G. Ciardelli, V. Chiono, Wound dressing products: a translational investigation from the bench to the market, Engineered Regeneration 3 (2) (2022) 182–200.
[4] G. Auriemma, P. Russo, P. Del Gaudio, C.A. García-González, M. Landín, R. P. Aquino, Technologies and formulation Design of Polysaccharide-Based Hydrogels for drug delivery, Molecules 25 (14) (2020) 3156.
[5] J. Jagur-Grodzinski, Polymeric gels and hydrogels for biomedical and pharmaceutical applications 21 (1) (2010) 27–47.
[6] C. Amante, V. Andretto, A. Rosso, G. Augusti, S. Marzocco, G. Lollo, P. Del Gaudio, Alginate-pectin microparticles loaded with nanoemulsions as nanocomposites for wound healing, Drug Deliv. Transl. Res. 13 (5) (2022) 1343–1357.
[7] J. Amirian, Y. Zeng, M.I. Shekh, G. Sharma, F.J. Stadler, J. Song, B. Du, Y. Zhu, In-situ crosslinked hydrogel based on amidated pectin/oxidized chitosan as potential wound dressing for skin repairing, Carbohydr. Polym. 251 (2021) 117005.
[8] C. Longinotti, The use of hyaluronic acid based dressings to treat burns: a review, Burns & Trauma 2 (4) (2014).
[9] P. Del Gaudio, C. Amante, R. Civale, V. Bizzarro, A. Petrella, G. Pepe, P. Campiglia, P. Russo, R.P. Aquino, In situ gelling alginate-pectin blend particles loaded with Ac2-26: a new weapon to improve wound care armamentarium, Carbohydr. Polym. 227 (2020) 115305.
[10] P. Makvandi, C. Caccavale, F. Della Sala, S. Zeppetelli, R. Veneziano, A. Borzacchiello, Natural formulations provide antioxidant complement to hyaluronic acid-based topical applications used in wound healing, Polymers 12 (8) (2020) 1847.
[11] A. Shamloo, Z. Aghababaie, H. Afjoul, M. Jami, M.R. Bidgoli, M. Vossoughi, A. Ramazani, K. Kamyabhesari, Fabrication and evaluation of chitosan/gelatin/PVA hydrogel incorporating honey for wound healing applications: an in vitro, in vivo study, Int. J. Pharm. 592 (2021) 120068.
[12] K.Y. Lee, D.J. Mooney, Alginate: properties and biomedical applications, Prog. Polym. Sci. 37 (1) (2012) 106–126.
[13] M.R. Sellitto, C. Amante, R.P. Aquino, P. Russo, R. Rodríguez-Dorado, M. Neagu, C. A. García-González, R. Adami, P. Del Gaudio, Hollow particles obtained by Prilling and supercritical drying as a potential conformable dressing for chronic wounds, Gels 9 (6) (2023) 492.
[14] M. Szekalska, A. Puciłowska, E. Szymańska, P. Ciosek, K. Winnicka, Alginate: current use and future perspectives in pharmaceutical and biomedical applications, International Journal of Polymer Science 2016 (2016) 7697031.
[15] R. Pereira, A. Tojeira, D.C. Vaz, A. Mendes, P. Bártolo, Preparation and characterization of films based on alginate and aloe Vera, Int. J. Polym. Anal. Charact. 16 (7) (2011) 449–464.
[16] H.E. Thu, M.H. Zulfakar, S.F. Ng, Alginate based bilayer hydrocolloid films as potential slow-release modern wound dressing, Int. J. Pharm. 434 (1–2) (2012) 375–383.
[17] F. De Cicco, A. Porta, F. Sansone, R.P. Aquino, P. Del Gaudio, Nanospray technology for an in situ gelling nanoparticulate powder as a wound dressing, Int. J. Pharm. 473 (1) (2014) 30–37.
[18] Q. Dang, K. Liu, C. Liu, T. Xu, J. Yan, F. Yan, D. Cha, Q. Zhang, Y. Cao, Preparation, characterization, and evaluation of 3, 6-ON-acetylethylenediamine modified chitosan as potential antimicrobial wound dressing material, Carbohydr. Polym. 180 (2018) 1–12.
[19] V. Davydova, A. Kalitnik, P. Markov, A. Volod'Ko, S. Popov, I. Ermak, Cytokine-inducing and anti-inflammatory activity of chitosan and its low-molecular derivative, Appl. Biochem. Microbiol. 52 (5) (2016) 476–482.
[20] H. Hattori, M. Ishihara, Changes in blood aggregation with differences in molecular weight and degree of deacetylation of chitosan, Biomed. Mater. 10 (1) (2015) 015014.
[21] J. Long, A.E. Etxeberria, A.V. Nand, C.R. Bunt, S. Ray, A. Seyfoddin, A 3D printed chitosan-pectin hydrogel wound dressing for lidocaine hydrochloride delivery, Mater. Sci. Eng. C Mater. Biol. Appl. 104 (2019) 109873.
[22] K. Nešović, A. Janković, T. Radetić, M. Vukašinović-Sekulić, V. Kojić, L. Živković, A. Perić-Grujić, K.Y. Rhee, V. Mišković-Stanković, Chitosan-based hydrogel wound dressings with electrochemically incorporated silver nanoparticles – in vitro study, Eur. Polym. J. 121 (2019) 109257.
[23] C. Amante, T. Esposito, P. Del Gaudio, V. Di Sarno, A. Porta, A. Tosco, P. Russo, L. Nicolais, R.P. Aquino, A novel three-polysaccharide blend in situ gelling powder for wound healing applications, Pharmaceutics 13 (10) (2021) 1680.
[24] C.E. Schanté, G. Zuber, C. Herlin, T.F. Vandamme, Chemical modifications of hyaluronic acid for the synthesis of derivatives for a broad range of biomedical applications, Carbohydr. Polym. 85 (3) (2011) 469–489.
[25] E. Nyman, J. Henricson, B. Ghafouri, C.D. Anderson, G. Kratz, Hyaluronic acid accelerates re-epithelialization and alters protein expression in a human wound model 7 (5) (2019) e2221.
[26] M. Prosdocimi, C. Bevilacqua, Exogenous hyaluronic acid and wound healing: an updated vision, Panminerva Med. 54 (2) (2012) 129–135.
[27] T.M. Tamer, M.N. Collins, K. Valachová, M.A. Hassan, A.M. Omer, M.S. Mohy-Eldin, K. Švík, R. Jurčík, Ľ. Ondruška, C. Biró, A.B. Albadarin, L. Šoltés, MitoQ loaded chitosan-hyaluronan composite membranes for wound healing 11 (4) (2018) 569.

[28] R.P. Aquino, G. Auriemma, T. Mencherini, P. Russo, A. Porta, R. Adami, S. Liparoti, G. Della Porta, E. Reverchon, P. Del Gaudio, Design and production of gentamicin/dextrans microparticles by supercritical assisted atomisation for the treatment of wound bacterial infections, Int. J. Pharm. 440 (2) (2013) 188–194.
[29] K. Ruckmani, S.Z. Shaikh, P. Khalil, M.S. Muneera, O.A. Thusleem, Determination of sodium hyaluronate in pharmaceutical formulations by HPLC–UV, Journal of Pharmaceutical Analysis 3 (5) (2013) 324–329.
[30] P.G. Bowler, S. Welsby, V. Towers, R. Booth, A. Hogarth, V. Rowlands, A. Joseph, S.A. Jones, Multidrug-resistant organisms, wounds and topical antimicrobial protection 9 (4) (2012) 387–396.
[31] J. Said, C.C. Dodoo, M. Walker, D. Parsons, P. Stapleton, A.E. Beezer, S. Gaisford, An in vitro test of the efficacy of silver-containing wound dressings against Staphylococcus aureus and Pseudomonas aeruginosa in simulated wound fluid, Int. J. Pharm. 462 (1) (2014) 123–128.
[32] G. Auriemma, P. Del Gaudio, A.A. Barba, M. d'Amore, R.P. Aquino, A combined technique based on prilling and microwave assisted treatments for the production of ketoprofen controlled release dosage forms, Int. J. Pharm. 415 (1) (2011) 196–205.
[33] L. Ren, B. Zhou, L. Chen, Silicone ring implantation in an excisional murine wound model, Wounds 24 (2) (2012) 36–42.
[34] H.D. Zomer, A.G. Trentin, Skin wound healing in humans and mice: challenges in translational research, J. Dermatol. Sci. 90 (1) (2018) 3–12.
[35] T. Li, B. Wan, R. Jog, A. Costa, D.J. Burgess, Pectin microparticles for peptide delivery: optimization of spray drying processing, Int. J. Pharm. 613 (2022) 121384.
[36] M. Mishra, B. Mishra, Formulation optimization and characterization of spray dried microparticles for inhalation delivery of doxycycline hyclate, Yakugaku Zasshi 131 (12) (2011) 1813–1825.
[37] G. Ma, Y. Liu, D. Fang, J. Chen, C. Peng, X. Fei, J. Nie, Hyaluronic acid/chitosan polyelectrolyte complexes nanofibers prepared by electrospinning, Mater. Lett. 74 (2012) 78–80.
[38] R.C. Polexe, T. Delair, Elaboration of Stable and antibody functionalized positively charged colloids by polyelectrolyte complexation between chitosan and hyaluronic acid 18 (7) (2013) 8563–8578.
[39] S. Honary, M. Maleki, M. Karami, The effect of chitosan molecular weight on the properties of alginate/chitosan microparticles containing prednisolone, Tropical Journal of Pharmaceutical Research (ISSN: 1596–5996) Vol 8 Num 1 8 (2009).
[40] F. Martinelli, A.G. Balducci, A. Kumar, F. Sonvico, B. Forbes, R. Bettini, F. Buttini, Engineered sodium hyaluronate respirable dry powders for pulmonary drug delivery, Int. J. Pharm. 517 (1) (2017) 286–295.
[41] D. Kulig, A. Zimoch-Korzycka, A. Jarmoluk, K. Marycz, Study on alginate–chitosan complex formed with different polymers ratio 8 (5) (2016) 167.
[42] C. Amante, G. Falcone, R.P. Aquino, P. Russo, L. Nicolais, P. Del Gaudio, In situ hydrogel formulation for advanced wound dressing: influence of co-solvents and functional excipient on tailored alginate-pectin-chitosan blend gelation kinetics, adhesiveness, and performance, Gels 10 (1) (2024) 3.
[43] R. Shi, T.L. Sun, F. Luo, T. Nakajima, T. Kurokawa, Y.Z. Bin, M. Rubinstein, J. P. Gong, Elastic–Plastic Transformation of Polyelectrolyte Complex Hydrogels from Chitosan and Sodium Hyaluronate, Macromolecules 51 (21) (2018) 8887–8898.
[44] S. Wu, L. Deng, H. Hsia, K. Xu, Y. He, Q. Huang, Y. Peng, Z. Zhou, C. Peng, Evaluation of gelatin-hyaluronic acid composite hydrogels for accelerating wound healing, J. Biomater. Appl. 31 (10) (2017) 1380–1390.
[45] T. Sagawa, M. Sakakibara, K. Iijima, Y. Yataka, M. Hashizume, Preparation and physical properties of free-standing films made of polyion complexes of carboxymethylated hyaluronic acid and chitosan, Polymer 253 (2022) 125033.
[46] H. Jung, M.K. Kim, J.Y. Lee, S.W. Choi, J. Kim, Adhesive hydrogel patch with enhanced strength and adhesiveness to skin for transdermal drug delivery, Adv. Funct. Mater. 30 (42) (2020) 2004407.
[47] Y. Kobayashi, A. Okamoto, K. Nishinari, Viscoelasticity of hyaluronic acid with different molecular weights, Biorheology 31 (1994) 235–244.
[48] G. Falcone, P. Mazzei, A. Piccolo, T. Esposito, T. Mencherini, R.P. Aquino, P. Del Gaudio, P. Russo, Advanced printable hydrogels from pre-crosslinked alginate as a new tool in semi solid extrusion 3D printing process, Carbohydr. Polym. 276 (2022) 118746.
[49] R. Deshmukh, R.K. Harwansh, S.D. Paul, R. Shukla, Controlled release of sulfasalazine loaded amidated pectin microparticles through Eudragit S 100 coated capsule for management of inflammatory bowel disease, Journal of Drug Delivery Science and Technology 55 (2020) 101495.
[50] J. Amirian, Y. Zeng, M.I. Shekh, G. Sharma, F.J. Stadler, J. Song, B. Du, Y. Zhu, In-situ crosslinked hydrogel based on amidated pectin/oxidized chitosan as potential wound dressing for skin repairing, Carbohydr. Polym. 251 (2021) 117005.
[51] K. Benešová, M. Pekař, L. Lapčík, J. Kučerík, Calorimetry, stability evaluation of n-alkyl hyaluronic acid derivates by DSC and TG measurement, J. Therm. Anal. Calorim. 83 (2) (2006) 341–348.
[52] N. Barroso, O. Guaresti, L. Pérez-Álvarez, L. Ruiz-Rubio, N. Gabilondo, J.L. Vilas-Vilela, Self-healable hyaluronic acid/chitosan polyelectrolyte complex hydrogels and multilayers, Eur. Polym. J. 120 (2019) 109268.
[53] X. Meng, Y. Lu, Y. Gao, S. Cheng, F. Tian, Y. Xiao, F. Li, Chitosan/alginate/hyaluronic acid polyelectrolyte composite sponges crosslinked with genipin for wound dressing application, Int. J. Biol. Macromol. 182 (2021) 512–523.
[54] J.A. Alkrad, Y. Mrestani, D. Stroehl, S. Wartewig, R. Neubert, Characterization of enzymatically digested hyaluronic acid using NMR, Raman, IR, and UV–vis spectroscopies, J. Pharm. Biomed. Anal. 31 (3) (2003) 545–550.
[55] J. Brugnerotto, J. Lizardi, F.M. Goycoolea, W. Argüelles-Monal, J. Desbrières, M. Rinaudo, An infrared investigation in relation with chitin and chitosan characterization, Polymer 42 (8) (2001) 3569–3580.
[56] T. Dai, M. Tanaka, Y.-Y. Huang, M.R. Hamblin, Chitosan preparations for wounds and burns: antimicrobial and wound-healing effects, Expert Rev. Anti Infect. Ther. 9 (7) (2011) 857–879.
[57] W.-R. Lee, J.-H. Park, K.-H. Kim, S.-J. Kim, D.-H. Park, M.-H. Chae, S.-H. Suh, S.-W. Jeong, K.-K. Park, The biological effects of topical alginate treatment in an animal model of skin wound healing, Wound Repair Regen. 17 (4) (2009) 505–510.
[58] Y. Kawano, V. Patrulea, E. Sublet, G. Borchard, T. Iyoda, R. Kageyama, A. Morita, S. Seino, H. Yoshida, O. Jordan, T. Hanawa, Wound healing promotion by hyaluronic acid: effect of molecular weight on gene expression and in vivo wound closure, Pharmaceuticals (Basel) 14 (4) (2021).